Chapter 6

Outlining impact of Hall currents on unsteady magneto-convection in a moving channel with Cogley-Vincent-Gilles heat flux model

6.1 Introduction

Magnetohydrodynamics (MHD) has emerged as a vibrant area of advanced engineering and applied mechanics. In 1942, Alfv́en [4] discovered the electromagnet-hydrodynamics waves which open a vast area of interest for scientists and researchers. This groundbreaking work of Alfv́en gains a lot of significance because it has many applications in every subfield of science specifically in geophysics, astrophysics, electrical engineering, mechanical engineering and aerospace engineering. The magnetohydrodynamic flow and heat transfer has attracted the attention of engineers, scientists, physicist and mathematicians in recent past owing to its cardinal significance in engineering and industrial applications such as MHD pumps, MHD power generators, MHD sensors, MHD flow meter, aerodynamic heating, electric transformers, electrostatic precipitation polymer technology, petroleum production, cooling of a metallic plate in a cooling bath, micro-mixing of physiological samples, biological transportation and drug delivery. MHD pumps are already in use in chemical energy technology for pumping

electrically conducting fluids at some of the atomic energy centers. An MHD generator is used to extract a portion of the aerodynamic heating energy from the inlet and an MHD accelerator is used to reintroduce this power as kinetic energy to the exhaust stream. The movement of an electrically conducting fluid in a magnetic filed is one of the main features of magnetohydrodynamics. MHD in the present form is due to pioneer contribution of several distinguished authors like Cowling [7], Shercliff [11], Ferraro and Plumpton [10], Gupta and Gupta [96], Datta and Jana [98], and Crammer and Pai [346]. Due to the varied range of applications in engineering and the universe, magnetohydrodynamic convection in channel has become significant. The radiative convective flows in channel and annulus under the effect of magnetic field are frequently encountered in many scientific and environmental processes such as astrophysical flows, water evaporation from open reservoirs, heating and cooling of chambers and solar power technology. The MHD flow and heat transfer by simultaneous thermal radiation and convection has applications in numerous technological problems including combustion, furnace design, nuclear reactor safety, fluidized bed heat exchanger, fire spreads, solar fans, solar collectors, manufacture of ceramics and glassware and smelting, turbid water bodies, photochemical reactors and many others. The free convection in channels has received attention among researchers in the last few decades due to its widespread importance in engineering applications like cooling of electronic equipment, design of passive solar systems for energy conversion, design of heat exchangers, human comfort in buildings, thermal regulation processes and many more. MHD natural convection flow of different fluids under different geometrical conditions in physical sense has been studied widely in the literature [347-353]. Jha et al. [109] have ascertained the fully developed natural convective flow of conducting fluid in a vertical microchannel under the influence of magnetic field. They have been reported that the increase in Hartmann number is responsible for reduction in the volume flow rate. VeeraKrishna and Reddy [354] have presented an unsteady MHD convective flow of second grade fluid through a channel filled with a porous medium in a rotating frame.

In partially ionized gases or fluids as such as electrolysis, salt water and solar wind, the phenomenon of Hall effects occurs when the intensity of the applied magnetic field is very strong or when the cyclotron frequency is high [355]. The current induced in fluid is usually carried mainly by electrons which undergo successive collisions with other charged or neutral particles and are usually more mobile than ions. As a result of these gyration and drift of charged particles, the conductivity parallel to the electric field is reduced and the current is induced in the direction normal to both electric and magnetic fields. This phenomenon generates an isotropic conductivity which is known as the Hall

current. The occurance of Hall current demands the modification of Ohm's law, also the consequences of this phenomenon enhance the order of flow goverened differential equations. The dimensionless product $\omega_e\tau_e$, typically called the Hall parameter, is an important characteristic number in the MHD design where ω_e is the electron cyclotron frequency and τ_e is the electron collision mean free time. On the microscopic scale, the Hall parameter be a sign of the average angular travel of electrons between collisions while on the macroscopic scale, the value of $\omega_e\tau_e$ signifies the relative importance of the Hall field and the Hall current. Hall currents significantly modify the flow dynamics in many cosmological objects such as dense molecular clouds and formation of white dwarfs. The importance of Hall current in electrically conducting fluid flows under the strong magnetic field has been emphasized by Lighthill [356]. Hall current has important engineering applications, such as Hall generators, Hall sensors, Hall probes, turbine, space missions and magnetic reconnection at the Earth's magnetopause [357].

Although there are many studies on MHD natural convective flow of an electrically conducting fluid in channels, there are only a few studies regarding MHD natural convection flow of an electrically conducting fluid in channels, annulus, microchannel and annular microchannel subject to a uniform strong magnetic field with Hall effects. Some authors have carried out a number of studies on MHD natural convection covering several aspects [358-368]. Pop et al. [369] have scrutinized the effect of Hall currents on free and forced convective flow in a rotating channel under the influence of an inclined magnetic field. Guria and Jana [68] have explored the Hall effects on the combined free and forced convective flow through a rotating channel in the presence of a uniform transverse magnetic field under general wall conditions. MHD convective flow in a rotating channel with Hall effects has been presented by Katagiri et al. [370]. Singh and Pathak [73] have inspected the effects of rotation and Hall currents on mixed convective MHD flow in a vertical channel filled with a porous medium. The MHD free convective flow in a vertical channel with an oscillatory wall temperature considering Hall currents has been analyzed by Guchhait et al. [134]. Zhang and Chen [371] have examined the Hall effects on natural convective MHD flow in a cavity. Das and Jana [107] have reported the Hall effects on unsteady free convection in a heated vertical channel. Guchhait et al. [84] have analyzed the Hall effects on an unsteady hydromagnetic free convective flow of a viscous incompressible electrically conducting fluid in the presence of an inclined magnetic field. An oscillatory unsteady MHD convective flow in a vertical channel filled with porous medium in the presence of Hall and thermal radiation effects have been studied by Das et al. [139]. Seth et al. [372] have explained combined free and forced convection Couette-Hartmann

flow of a viscous, incompressible and electrically conducting fluid in rotating channel with arbitrary conducting walls in the presence of Hall current. Jha et al. [114] have examined the Hall effects on the steady fully developed magnetohydrodynamic natural convective flow in a vertical microchannel with asymmetric heating. VeeraKrishna et al. [373] have inspected the effects of Hall currents on unsteady MHD oscillatory free convective flow of second grade fluid in vertical channel through porous medium.

In this chapter, our main concern is to discourse the impact of Hall current effects on the MHD convective flow of a viscous incompressible electrically conducting fluid in a moving vertical channel along with Cogley-Vincent-Gilles heat flux theory. The heat due to viscous and Joule dissipations and the induced magnetic field is assumed to be neglected. The magnetic Reynolds number is assumed very small for the partially-ionized fluid so that magnetic induction effects can be ignored [355]. The relative motion of the charged particles in the fluid can occur and the electron-atom collision frequency is assumed to be high enough for Hall currents to be significant. An electric current density is required to represent the relative motion of charged particles. The momentum and energy equations are solved by the Laplace transform technique. Analytical closed form solutions are obtained. In order to obtain clear insight of physical phenomenon in the channel, the interested quantities viz. velocity and temperature profiles, shear stresses, rate of heat transfer for different pertinent parameters are plotted graphically with the help of MATLAB software and discussed under different intricate physical parameters. The results obtained in this chapter are consistent with the physical situation of the problem.

6.2 Mathematical model

Consider the unsteady flow and heat transfer of a viscous incompressible electrically conducting fluid between two infinite vertical parallel plates separated by a distance h, which is small compared to the characteristic lengths of the channel walls. A Cartesian co-ordinates system with the x-axis along left wall of the channel vertically upward direction, y-axis normal to the channel walls and z-axis perpendicular to xy-plane is introduced (see Fig.6.1). Initially, at time $t \leq 0$, both the fluid and plates are assumed to be at rest with a constant temperature T_h. At time $t > 0$, the right wall at $y = h$ starts to move with a velocity $U(t)$ in its own plane and the temperature of the moving wall is instantaneously raised or lowered to T_h and that is maintained for all time, t being the time, while the left wall at $y = 0$ is kept fixed and the temperature is assumed to be of constant value T_0. A uniform strong magnetic field of strength B_0

is imposed parallel to the y-axis. As the channel walls are of infinite extent in the x and z-directions and electrically non-conducting, all physical quantities are function of y and t only. The effect of Hall current gives rise to a force in the z-direction, which induces a cross flow in that direction and hence the flow becomes two dimensional. To simplify the analysis, we assume that there is no variation of flow quantities in the z-direction which is valid if the plates would be of infinite width in this direction. To simplify the analysis, it is assumed that the Joule heating and viscous dissipation are neglected in this work. Further, the fluid is assumed to be isotropic and homogeneous and has the scalar constant viscosity and electric conductivity.

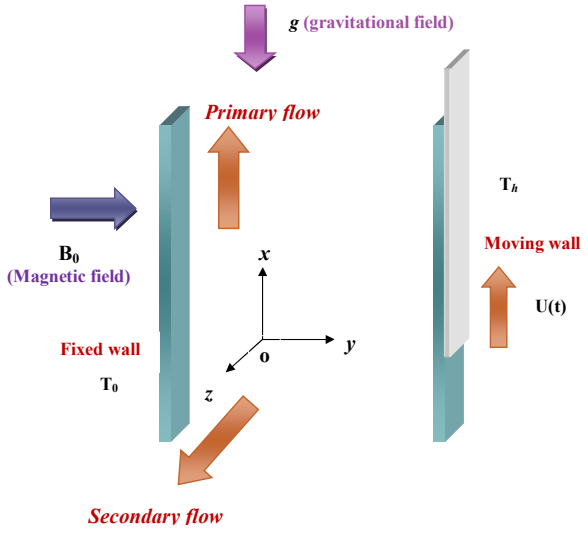

Fig.6.1 : *Physical configuration*

In view of above assumptions, the momentum and energy equations which govern the free convective flow of a viscous incompressible electrically conducting fluid in a vertical channel on taking thermal radiation into account under usual Boussinesq's approximation are as follows [84]

$$\frac{\partial u}{\partial t} = \nu \frac{\partial^2 u}{\partial y^2} + g\beta(T - T_h) - \frac{B_0}{\rho} j_z, \tag{6.1}$$

$$\frac{\partial w}{\partial t} = \nu \frac{\partial^2 w}{\partial y^2} + \frac{B_0}{\rho} j_x, \tag{6.2}$$

$$\rho c_p \frac{\partial T}{\partial t} = k \frac{\partial^2 T}{\partial y^2} - \frac{\partial q_r}{\partial y}, \tag{6.3}$$

where u and w are the velocity components in the x and z-direction, respectively, j_x and j_z are components of current density in the x and z-direction, respectively, T the fluid

temperature, t the time, g the gravitational acceleration, β the coefficient of thermal expansion, ρ the fluid density, ν the kinematic viscosity, k the thermal conductivity, c_p the specific heat at constant pressure, q_r the radiative heat flux in the y-direction and the term $\frac{\partial q_r}{\partial y}$ represents the change in the radiative heat flux with distance normal to the channel.

The appropriate initial and boundary conditions for the flow in the moving channel are prescribed as follows [350]

$$\begin{aligned} &t \leq 0 : u = w = 0, \;\; T = T_h \;\text{ for all }\; 0 \leq y \leq h, \\ &t > 0 : u = w = 0, \;\; T = T_0 \;\text{ at }\; y = 0, \\ &t > 0 : u = U(t), \;\; w = 0, \;\; T = T_h \;\text{ at }\; y = h. \end{aligned} \tag{6.4}$$

The generalized Ohm's law with Hall current effects takes the following form (Cowling [7])

$$\vec{j} + \frac{\omega_e \tau_e}{B_0}\left(\vec{j} \times \vec{B}\right) = \sigma(\vec{E} + \vec{q} \times \vec{B}), \tag{6.5}$$

where $\vec{q} = (u, 0, w)$ is the velocity vector, $\vec{j} = (j_x, j_y, j_z)$ the currents density vector, $\vec{B} = (B_x, B_y, B_z)$ the magnetic field vector, $\vec{E} = (E_x, E_y, E_z)$ the electric field vector, σ the electrical conductivity, ω_e the cyclotron frequency and τ_e the collision time of electron.

In writing (6.5), the ion-slip and the thermoelectric effects as well as the electron pressure gradient are neglected which is justified for partially ionized gas. The right hand side within the bracket is the electric field in the moving frame. The first term on the left hand side comes from the electron drag on the ions. The second term is the Hall term and has to do with the idea that electrons and ions can decouple and move separately. In case of electrically conducting fluid, the flow and heat transfer are induced by an imposed magnetic field. An electromotive force (or emf) is produced in the fluid flowing across the transverse magnetic field. The resultant effect of current and magnetic field produces a force, resisting the fluid motion. The fluid velocity also affects the magnetic field by producing an induced magnetic field which perturbs the original field. The Hall current effect is the direct result of the Lorentz force $\vec{j} \times \vec{B}$. The Lorentz force is that which governs the behavior of charged particles in a magnetic field. It is that force which accounts for the deflection of electron beams in magnetically deflected cathode ray tubes and the rotation of electric motor armatures. Further, it is assumed that $\omega_e \, \tau_e \sim O(1)$ and $\omega_i \, \tau_i \ll 1$, where ω_e, ω_i are the cyclotron frequency of electrons and ions and τ_e, τ_i are the collision time for electrons and ions, respectively.

The solenoidal relation $\nabla \cdot \vec{B} = 0$ for the magnetic field gives $B_y = B_0 =$ constant everywhere in the fluid i.e. $\vec{B} \equiv (0, B_0, 0)$. The equation of conservation of the charge $\nabla \cdot \vec{j} = 0$ gives $j_y =$ constant, where (j_x, j_y, j_z) are the components of the currents density $\vec{j}$. This constant is zero since $j_y = 0$ at the plates which are electrically non-conducting. Thus $j_y = 0$ everywhere in the flow field. So $\vec{j} \equiv (j_x, 0, j_z)$. Since the induced magnetic field is neglected, the Maxwell's equation $\nabla \times \vec{E} = -\frac{\partial \vec{B}}{\partial t}$ becomes $\nabla \times \vec{E} = 0$ which gives $\frac{\partial E_z}{\partial y} = 0$ and $\frac{\partial E_x}{\partial y} = 0$. This implies that $E_x =$ constant and $E_z =$ constant everywhere in the flow.

Assuming $E_x = 0$ and $E_z = 0$, the equation (6.5) yields

$$j_x - m\, j_z = -\sigma w B_0, \tag{6.6}$$

$$j_z + m\, j_x = \sigma u B_0, \tag{6.7}$$

where $m = \omega_e \tau_e$ is the Hall parameter. The effect of Hall current gives rise to a force in the z-direction, which induces a cross flow in that direction and hence the flow becomes two dimensional. To simplify the problem, we assume that there is no variation of flow quantities in z-direction. This assumption is considered to be valid if the surface be of infinite extent in the z-direction.

On solving equations (6.6) and (6.7), we have

$$j_x = \frac{\sigma B_0}{1+m^2}\,(mu - w)\,, \tag{6.8}$$

$$j_z = \frac{\sigma B_0}{1+m^2}\,(mw + u)\,. \tag{6.9}$$

On the use of (6.8) and (6.9), equations (6.1) and (6.2) reduce to

$$\frac{\partial u}{\partial t} = \nu \frac{\partial^2 u}{\partial y^2} - \frac{\sigma B_0^2}{\rho(1+m^2)}\,(mw + u) + g\beta\,(T - T_h)\,, \tag{6.10}$$

$$\frac{\partial w}{\partial t} = \nu \frac{\partial^2 w}{\partial y^2} - \frac{\sigma B_0^2}{\rho(1+m^2)}\,(w - mu)\,. \tag{6.11}$$

The flow described by equations (6.10) and (6.11) are the general representation of the velocity distribution for the flow through a vertical channel of any conducting medium due to the movement of the right wall in the presence of free convective currents.

The optically thin assumption is worth noting since most investigations have utilized it when dealing with gases. Following Cogley et al. [192], in the optically thin limit for a non-grey gas near equilibrium situation, the following relation holds

$$\frac{\partial q_r}{\partial y} = 4(T - T_h) \int_0^\infty K_{\lambda_w} \left[\frac{\partial e_{\lambda_p}(T)}{\partial T}\right]_w d\lambda, \tag{6.12}$$

where K_{λ_w} is the frequency-dependent absorption coefficient at the wall, λ is the wave length, $e_{\lambda_p}(T)$ is the Planck's function and subscript w denotes that all quantities have been evaluated at the reference temperature T_h which is the temperature of the right wall of the channel at time $t \leq 0$. Thus, our study is limited to small difference of plate temperature to the fluid temperature.

Substituting (6.12) in (6.3), we obtain

$$\rho c_p \frac{\partial T}{\partial t} = k \frac{\partial^2 T}{\partial y^2} - 4\,(T - T_h)\,I, \tag{6.13}$$

where

$$I = \int_0^\infty K_{\lambda_w} \left[\frac{\partial e_{\lambda_p}(T)}{\partial T}\right]_w d\lambda. \tag{6.14}$$

Introducing the non-dimensional variables

$$\eta = \frac{y}{h},\;\; u_1 = \frac{u}{U_0},\;\; w_1 = \frac{w}{U_0},\;\; \theta = \frac{T - T_h}{T_0 - T_h},\;\; \tau = \frac{\nu t}{h^2},\;\; U(t) = U_0 f(\tau) \tag{6.15}$$

equations (6.10), (6.11) and (6.13) become

$$\frac{\partial u_1}{\partial \tau} = \frac{\partial^2 u_1}{\partial \eta^2} - \frac{M^2}{(1+m^2)}\,(u_1 + m w_1) + Gr\;\theta, \tag{6.16}$$

$$\frac{\partial w_1}{\partial \tau} = \frac{\partial^2 w_1}{\partial \eta^2} - \frac{M^2}{(1+m^2)}\,(w_1 - m u_1)\,, \tag{6.17}$$

$$Pr \frac{\partial \theta}{\partial \tau} = \frac{\partial^2 \theta}{\partial \eta^2} - N\;\theta, \tag{6.18}$$

where $M^2 = \frac{\sigma B_0^2 h^2}{\nu \rho}$ is the squared-Hartmann number which may be interpreted as the ratio of induction drag to viscous drag, $Gr = \frac{g\beta(T_0 - T_h)h^2}{\nu U_0}$ the Grashof number which signifies the relative strength of the thermal buoyancy force to the viscous force, $Pr = \frac{\nu \rho c_p}{k}$ the Prandtl number which defines the relative effectiveness of momentum and energy transport by diffusion i.e. the ratio of momentum to thermal diffusivity in the ionized fluid, $N = \frac{4Ih^2}{k}$ the radiation parameter, $f(\tau)$ a known function and U_0 being a constant.

It is convenient to combine equations (6.16) and (6.17) into a single equation. We multiply equation (6.17) by i and add the resultant to equation (6.16) to obtain

$$\frac{\partial q}{\partial \tau} = \frac{\partial^2 q}{\partial \eta^2} - a\,q + Gr\,\theta, \tag{6.19}$$

where $q(= u_1 + i\,w_1)$ is the fluid velocity in the complex form, $a = M^2(1 - i\,m)/(1 + m^2)$ and $i = \sqrt{-1}$.

The initial and boundary conditions for $q(\eta)$ and $\theta(\eta)$ can be put in the following form

$$\begin{aligned} &\tau \leq 0 : q = 0, \;\; \theta = 0 \;\text{ for all }\; \eta, \\ &\tau > 0 : q = 0, \;\; \theta = 1 \;\text{ at }\; \eta = 0, \\ &\tau > 0 : q = f(\tau), \;\; \theta = 0 \;\text{ at }\; \eta = 1. \end{aligned} \tag{6.20}$$

The exact solution of (6.18) and (6.19) with initial and boundary conditions (6.20) can be obtained by using the Laplace transform technique. On taking Laplace transform of (6.18) and (6.19), we have

$$\frac{d^2\bar{\theta}}{d\eta^2} - (sPr + N)\,\bar{\theta} = 0, \tag{6.21}$$

$$\frac{d^2\bar{q}}{d\eta^2} - (s + a)\,\bar{q} + Gr\,\bar{\theta} = 0, \tag{6.22}$$

where

$$\bar{q}(\eta, s) = \int_0^\infty q(\eta, \tau)\, e^{-s\tau}\, d\tau, \;\; \bar{\theta}(\eta, s) = \int_0^\infty \theta(\eta, \tau)\, e^{-s\tau}\, d\tau, \tag{6.23}$$

and $s(> 0)$ is the Laplace transform variable.

The corresponding boundary conditions are

$$\bar{q}(0, s) = 0, \;\; \bar{\theta}(0, s) = \frac{1}{s}, \;\; \bar{q}(1, s) = \bar{f}(s), \;\; \bar{\theta}(1, s) = 0, \tag{6.24}$$

where $\bar{f}(s)$ is the Laplace transform of the function $f(\tau)$.

The solution of equations (6.21) and (6.22) subject to the boundary conditions (6.24) are

$$\bar{\theta}(\eta, s) = \frac{1}{s}\frac{\sinh\sqrt{sPr + N}(1 - \eta)}{\sinh\sqrt{sPr + N}}, \tag{6.25}$$

$$\begin{aligned} \bar{q}(\eta, s) &= \bar{f}(s)\frac{\sinh\sqrt{s + a}\;\eta}{\sinh\sqrt{s + a}} + \frac{Gr}{(Pr - 1)}\frac{1}{s(s + \alpha)}\left[\frac{\sinh\sqrt{s + a}(1 - \eta)}{\sinh\sqrt{s + a}}\right. \\ &- \left.\frac{\sinh\sqrt{sPr + N}(1 - \eta)}{\sinh\sqrt{sPr + N}}\right], \end{aligned} \tag{6.26}$$

where $\alpha = \frac{N - a}{Pr - 1}$.

We obtain the temperature distribution $\theta(\eta,\tau)$ on taking the Laplace inversion of (6.25) as

$$\theta(\eta,\tau) = \begin{cases} \frac{\sinh\sqrt{N}(1-\eta)}{\sinh\sqrt{N}} - 2\pi\sum_{n=1}^{\infty}\frac{e^{-\left(N+n^2\pi^2\right)\frac{\tau}{Pr}}}{(N+n^2\pi^2)}\, n\sin n\pi\eta & \text{for } Pr\neq 1 \\ \frac{\sinh\sqrt{N}(1-\eta)}{\sinh\sqrt{N}} - 2\pi\sum_{n=1}^{\infty}\frac{e^{-\left(N+n^2\pi^2\right)\tau}}{(N+n^2\pi^2)}\, n\sin n\pi\eta & \text{for } Pr=1. \end{cases} \tag{6.27}$$

In this paper, we propose to investigate the following cases corresponding to the type of motions of the right wall of the channel.

6.2.1 Impulsive motion of right wall

For impulsive motion of the right wall of the channel, $f(\tau)=1$. Then $\bar{f}(s)=\frac{1}{s}$. The inverse Laplace transform of the equation (6.26) gives the expression of the complex fluid velocity $q(\eta,\tau)$ as

$$q(\eta,\tau) = \begin{cases} \frac{\sinh\sqrt{a}\ \eta}{\sinh\sqrt{a}} + \frac{Gr}{(Pr-1)\alpha}\left\{\frac{\sinh\sqrt{a}(1-\eta)}{\sinh\sqrt{a}} - \frac{\sinh\sqrt{N}(1-\eta)}{\sinh\sqrt{N}}\right\} \\ +2\sum_{n=1}^{\infty} n\pi\left[(-1)^n\,\frac{e^{-\left(a+n^2\pi^2\right)\tau}}{(a+n^2\pi^2)} + \frac{Gr}{Pr-1}\left\{\frac{e^{-\left(a+n^2\pi^2\right)\tau}}{(a+n^2\pi^2)(a-\alpha+n^2\pi^2)}\right.\right. \\ \left.\left. - \frac{e^{-\left(N+n^2\pi^2\right)\frac{\tau}{Pr}}}{(N+n^2\pi^2)\left\{\frac{1}{Pr}(N+n^2\pi^2)-\alpha\right\}}\right\}\right]\sin n\pi\eta & \text{for } Pr\neq 1 \\ \frac{\sinh\sqrt{a}\ \eta}{\sinh\sqrt{a}} + \frac{Gr}{(N-a)}\left\{\frac{\sinh\sqrt{a}(1-\eta)}{\sinh\sqrt{a}} - \frac{\sinh\sqrt{N}(1-\eta)}{\sinh\sqrt{N}}\right\} \\ +2\sum_{n=1}^{\infty} n\pi\left[\left\{(-1)^n - \frac{Gr}{N-a}\right\}\frac{e^{-\left(a+n^2\pi^2\right)\tau}}{(a+n^2\pi^2)}\right. \\ \left. + \frac{Gr}{N-a}\,\frac{e^{-\left(N+n^2\pi^2\right)\tau}}{(N+n^2\pi^2)}\right]\sin n\pi\eta & \text{for } Pr=1. \end{cases} \tag{6.28}$$

Equation (6.28) represents the unified expression for complex velocity of an electrically conducting fluid due to the impulsive motion of the right wall of the channel in the presence of strong magnetic filed with Hall current effects. Separating into a real and imaginary parts, one can easily obtain the non-dimensional velocity components u_1 and w_1 from (6.28).

The expression for the steady state complex velocity q_s is obtained by letting $\tau\to\infty$

in (6.28) as

$$q_s(\eta) = \begin{cases} \frac{\sinh\sqrt{a}\ \eta}{\sinh\sqrt{a}} + \frac{Gr}{(Pr-1)\alpha}\left\{\frac{\sinh\sqrt{a}(1-\eta)}{\sinh\sqrt{a}} - \frac{\sinh\sqrt{N}(1-\eta)}{\sinh\sqrt{N}}\right\} & \text{for } Pr \neq 1 \\ \frac{\sinh\sqrt{a}\ \eta}{\sinh\sqrt{a}} + \frac{Gr}{(N-a)}\left\{\frac{\sinh\sqrt{a}(1-\eta)}{\sinh\sqrt{a}} - \frac{\sinh\sqrt{N}(1-\eta)}{\sinh\sqrt{N}}\right\} & \text{for } Pr = 1. \end{cases} \tag{6.29}$$

6.2.2 Accelerated motion of right wall

In case of accelerated motion of the right wall of the channel, $f(\tau) = \tau$. Then $\bar{f}(s) = \frac{1}{s^2}$. On taking inverse Laplace transform of equation (6.26), we obtain the complex velocity $q(\eta, \tau)$ and expressed as

$$q(\eta,\tau) = \begin{cases} \frac{\sinh\sqrt{a}\ \eta}{\sinh\sqrt{a}}\ \tau + \frac{Gr}{(Pr-1)\alpha}\left\{\frac{\sinh\sqrt{a}(1-\eta)}{\sinh\sqrt{a}} - \frac{\sinh\sqrt{N}(1-\eta)}{\sinh\sqrt{N}}\right\} \\ +\frac{1}{2\sqrt{a}\sinh\sqrt{a}}\left(\eta\cosh\sqrt{a}\,\eta - \coth\sqrt{a}\sinh\sqrt{a}\,\eta\right) \\ -2\sum\limits_{n=1}^{\infty} n\pi\left[(-1)^n\ \frac{e^{-\left(a+n^2\pi^2\right)\tau}}{(a+n^2\pi^2)^2} - \frac{Gr}{Pr-1}\left\{\frac{e^{-\left(a+n^2\pi^2\right)\tau}}{(a+n^2\pi^2)(a-\alpha+n^2\pi^2)}\right.\right. \\ \left.\left. - \frac{Pr\,e^{-\left(N+n^2\pi^2\right)\frac{\tau}{Pr}}}{(N+n^2\pi^2)\{(N+n^2\pi^2)-\alpha\,Pr\}}\right\}\right]\sin n\pi\eta & \text{for } Pr \neq 1 \\ \frac{\sinh\sqrt{a}\,\eta}{\sinh\sqrt{a}}\ \tau + \frac{Gr}{(N-a)}\left\{\frac{\sinh\sqrt{a}(1-\eta)}{\sinh\sqrt{a}} - \frac{\sinh\sqrt{N}(1-\eta)}{\sinh\sqrt{N}}\right\} \\ +\frac{1}{2\sqrt{a}\sinh\sqrt{a}}\left(\eta\cosh\sqrt{a}\,\eta - \coth\sqrt{a}\sinh\sqrt{a}\,\eta\right) \\ -2\sum\limits_{n=1}^{\infty} n\pi\left[(-1)^n\ \frac{e^{-\left(a+n^2\pi^2\right)\tau}}{(a+n^2\pi)^2}\right. \\ \left. + \left\{\frac{e^{-\left(a+n^2\pi^2\right)\tau}}{(a+n^2\pi^2)} + \frac{Gr}{N-a}\ \frac{e^{-\left(N+n^2\pi^2\right)\tau}}{(N+n^2\pi^2)}\right\}\right]\sin n\pi\eta & \text{for } Pr = 1. \end{cases} \tag{6.30}$$

Equation (6.30) gives the unified expression for complex velocity of an electrically conducting fluid due to the accelerated motion of the right wall of the channel in the presence of strong magnetic filed with Hall effects. Separating into a real and imaginary parts one can easily obtain the non-dimensional velocity components u_1 and w_1 from (6.30).

For large time, i.e. $\tau \gg 1$, the equation (6.30) becomes

$$\tilde{q}(\eta) = \begin{cases} \frac{\sinh\sqrt{a}\ \eta}{\sinh\sqrt{a}}\ \tau + \frac{Gr}{(Pr-1)\alpha}\left\{\frac{\sinh\sqrt{a}(1-\eta)}{\sinh\sqrt{a}} - \frac{\sinh\sqrt{N}(1-\eta)}{\sinh\sqrt{N}}\right\} \\ +\frac{1}{2\sqrt{a}\sinh\sqrt{a}}\left(\eta\cosh\sqrt{a}\ \eta - \coth\sqrt{a}\sinh\sqrt{a}\ \eta\right) \qquad \text{for } Pr \neq 1 \\ \frac{\sinh\sqrt{a}\ \eta}{\sinh\sqrt{a}}\ \tau + \frac{Gr}{(N-a)}\left\{\frac{\sinh\sqrt{a}(1-\eta)}{\sinh\sqrt{a}} - \frac{\sinh\sqrt{N}(1-\eta)}{\sinh\sqrt{N}}\right\} \\ +\frac{1}{2\sqrt{a}\sinh\sqrt{a}}\left(\eta\cosh\sqrt{a}\ \eta - \coth\sqrt{a}\sinh\sqrt{a}\ \eta\right) \qquad \text{for } Pr = 1. \end{cases} \tag{6.31}$$

6.3 Results and discussion

The present chapter is a speculative investigation of the modelled problem addressing Hall current effects on MHD convective flow in a moving channel with Cogley-Vincent-Gilles heat flux theory. This section deals with the effects of various pertinent parameters, viz. squared-Hartmann number M^2, Hall parameter m, radiation parameter N, Grashof number Gr, Prandtl number Pr and time τ on the non-dimensional fluid velocity components, temperature profiles, shear stresses and rate of heat transfer. For this purpose, computations have been performed for the MHD flow with $M^2 = 10$, $m = 0.5$, $Gr = 5$, $N = 2$, $Pr = 0.71$, $\tau = 0.5$. For the whole investigation, these values are kept constant except the varying parameter which is presented in the respective figure. Physically, this data applies to electrically conducting electrolytic(water) solution, encountered in geophysical flows. It is noted that solutions given by (6.27), (6.28) and (6.30) satisfy all the imposed boundary conditions which provide a useful mathematical check of the results of the present study. The validity of calculated solutions of this study is ensured.

6.3.1 Primary and secondary velocity profiles

Figs.6.2(a) and 6.2(b) are sketched to expose the impact of squared-Hartmann number M^2 on the velocity components. The primary velocity significantly reduces for both cases of the impulsive and accelerated motions when M^2 is intensified[Fig.6.2(a)]. In

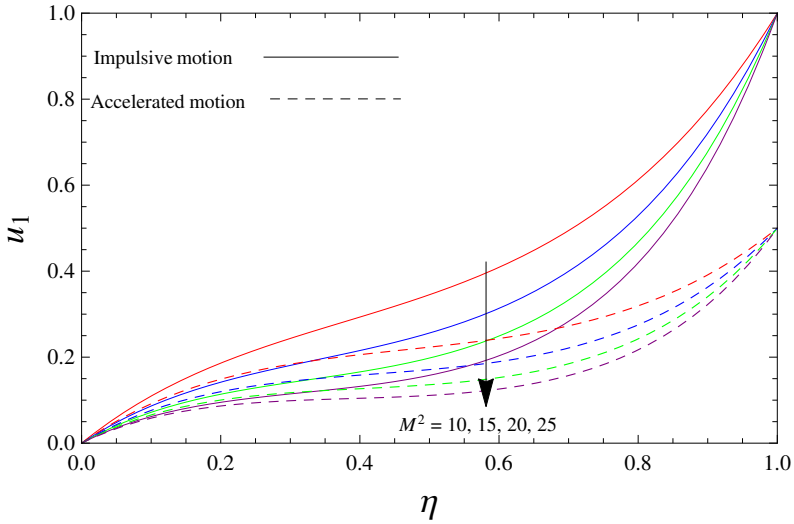

Fig.6.2(a): *Primary velocity profiles* u_1 *varying* M^2 *when* $N = 2$, $m = 0.5$, $Gr = 5$, $Pr = 0.71$ *and* $\tau = 0.5$

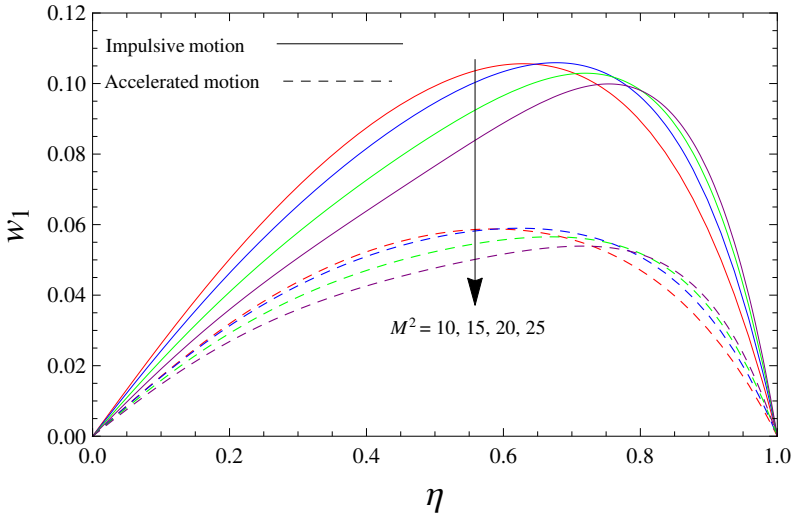

Fig.6.2(b): *Secondary velocity profiles* w_1 *varying* M^2 *when* $N = 2$, $m = 0.5$, $Gr = 5$, $Pr = 0.71$ *and* $\tau = 0.5$

Fig.6.2(b), the secondary velocity is observed to decrease with increasing M^2 in the vicinity of the left(fixed) wall of the channel and increases near the right(moving) wall of the channel for both type of motions. That is the primary or secondary fluid motion is significantly influenced due to application of transverse magnetic field. This is due to the related fact that the strength of strong magnetic field is responsible to generate the Lorentz force(an opposing force) in the flow field which opposes the fluid transport due to increasing Hartmann number. The secondary velocity is observed to be skewed towards the moving wall with gaining strength of magnetic field. The effect of

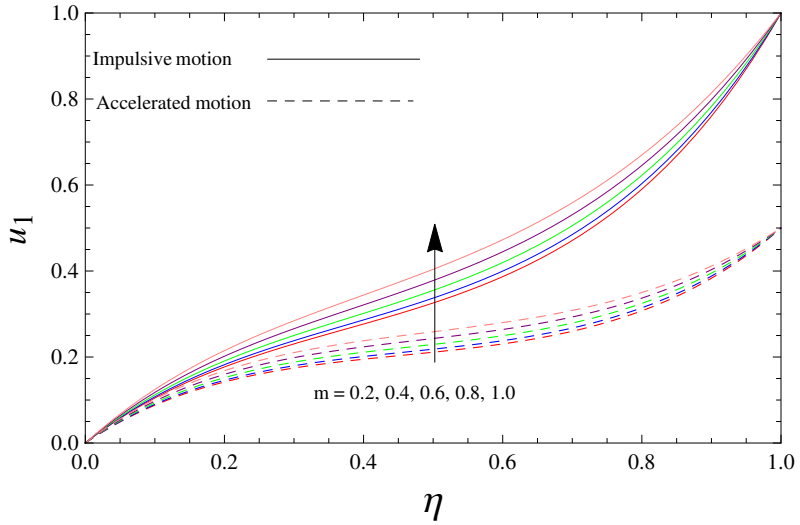

Fig.6.2(c): *Primary velocity profiles* u_1 *varying* m *when* $N = 2$, $M^2 = 10$, $Gr = 5$, $Pr = 0.71$ *and* $\tau = 0.5$

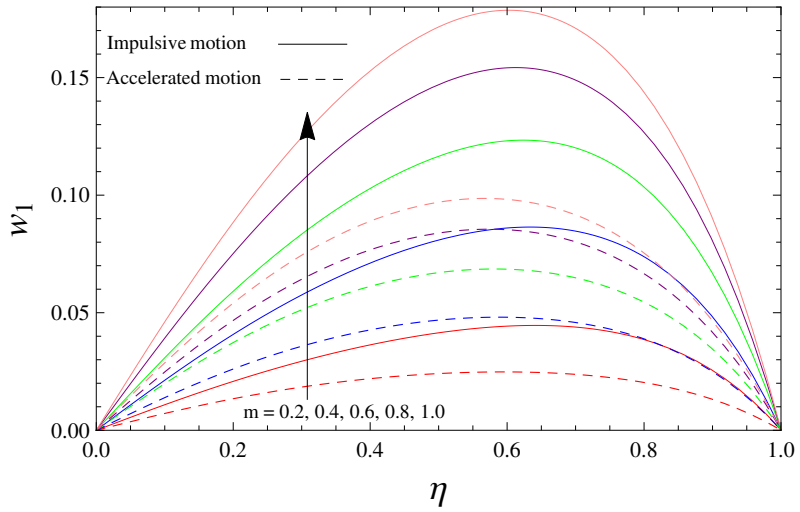

Fig.6.2(d): *Secondary velocity profiles* w_1 *varying* m *when* $N = 2$, $M^2 = 10$, $Gr = 5$, $Pr = 0.71$ *and* $\tau = 0.5$

Hall parameter m on the velocity components is depicted in Figs.6.2(c) and 6.2(d). As Hall parameter m increases, both the fluid velocity components enhance for both prescribed motions. Because increasing values of Hall parameter correspond to reduce in damping magnetic force and as a result motion of fluid is accelerated. This is a new phenomenon which appears as a result of imposing Hall current in the flow distribution. With increasing Hall parameter, the peak of secondary velocity is displaced closer to the right wall of the channel. This does not occur for the primary velocity. Figs.6.2(e)

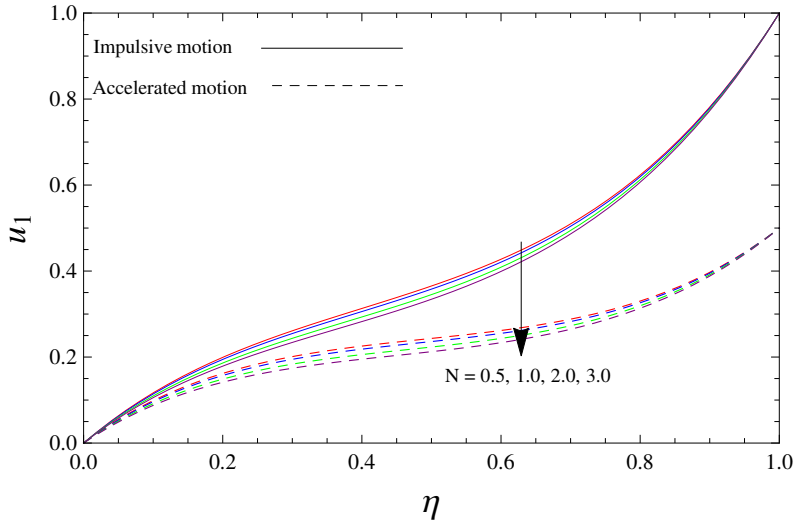

Fig.6.2(e): *Primary velocity profiles* u_1 *varying* N *when* $m = 0.5$, $M^2 = 10$, $Gr = 5$, $Pr = 0.71$ *and* $\tau = 0.5$

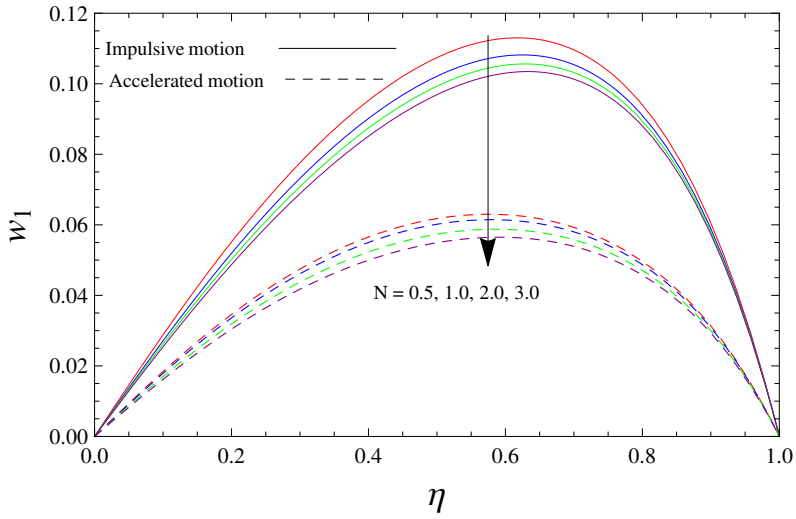

Fig.6.2(f): *Secondary velocity profiles* w_1 *varying* N *when* $m = 0.5$, $M^2 = 10$, $Gr = 5$, $Pr = 0.71$ *and* $\tau = 0.5$

and 6.2(f) expose the radiation parameter consequences on velocity components for both motions. These graphs explicate that both the velocity components are decreasing in nature against radiation parameter N. The presence of thermal radiation therefore clearly inhibits the primary as well as secondary flows. The thermal radiation has a significant effect on momentum in the flow system and provides a good mechanism for flow control. Figs.6.2(g) and 6.2(h) are chalked out to illustrate the influence of Grashof

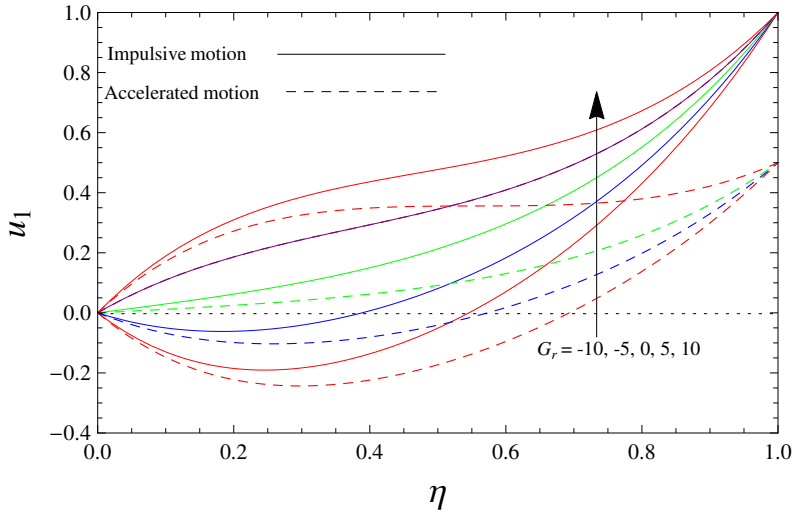

Fig.6.2(g): *Primary velocity profiles* u_1 *varying* Gr *when* $N = 2$, $m = 0.5$, $M^2 = 10$, $Pr = 0.71$ *and* $\tau = 0.5$

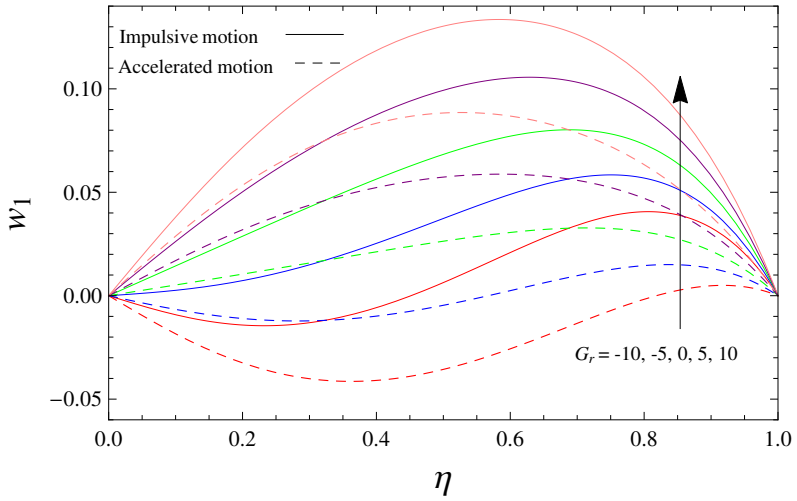

Fig.6.2(h): *Secondary velocity profiles* w_1 *varying* Gr *when* $N = 2$, $m = 0.5$, $M^2 = 10$, $Pr = 0.71$ *and* $\tau = 0.5$

number Gr on the velocity components. As demonstrated in these figures, both the velocity components are considerably boosted up due to a rise in Grashof number Gr for both type of motions of the right wall. The Grashof number signifies the ratio of buoyant force to viscous force and $Gr > 0$ leads to the situation when buoyant force is dominant and positive and flow is assisted by this force while $Gr < 0$ is the case when buoyant force is negative and opposes the flow. Both the primary and secondary velocities are negative for negative values of Grashof number, indicating that backflow occurs near the left wall of the channel. The magnitude of backflow is larger in case of accelerated motion. The maximum of the secondary velocity profiles shifts toward the

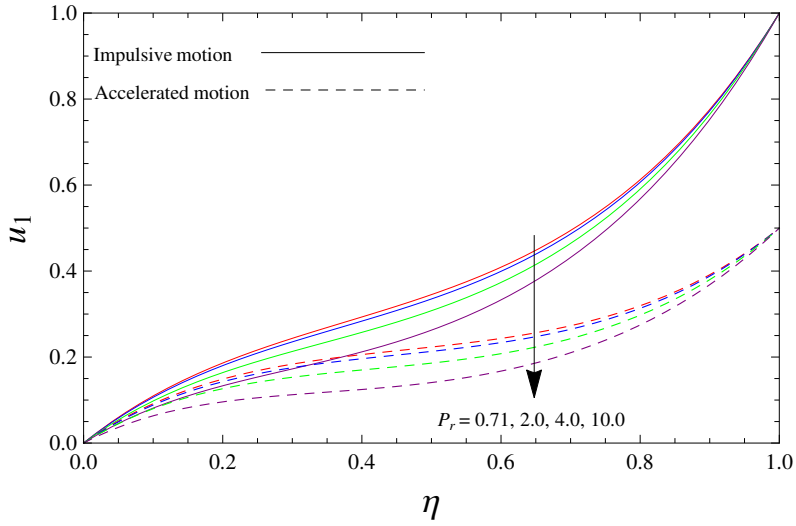

Fig.6.2(i): *Primary velocity profiles* u_1 *varying* Pr *when* $N = 2$, $m = 0.5$, $M^2 = 10$, $Gr = 5$ *and* $\tau = 0.5$

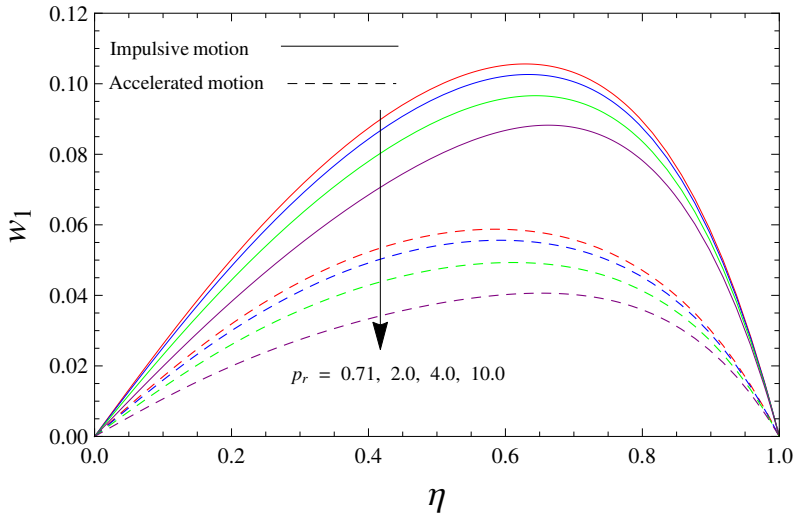

Fig.6.2(j): *Secondary velocity profiles* w_1 *varying* Pr *when* $N = 2$, $m = 0.5$, $M^2 = 10$, $Gr = 5$ *and* $\tau = 0.5$

right half of the channel due to the moving wall which is more hotter than the stationary wall. Figs.6.2(i) and 6.2(j) reflect that the velocity components are observed to decrease with increasing Prandtl number Pr for both cases of impulsive as well as accelerated motions of the right wall of the channel. Physically, this is quite true because an increase in the Prandtl number is due to increase in the viscosity of the fluid which makes the fluid thick and hence causes a decrease in the fluid velocity components. From

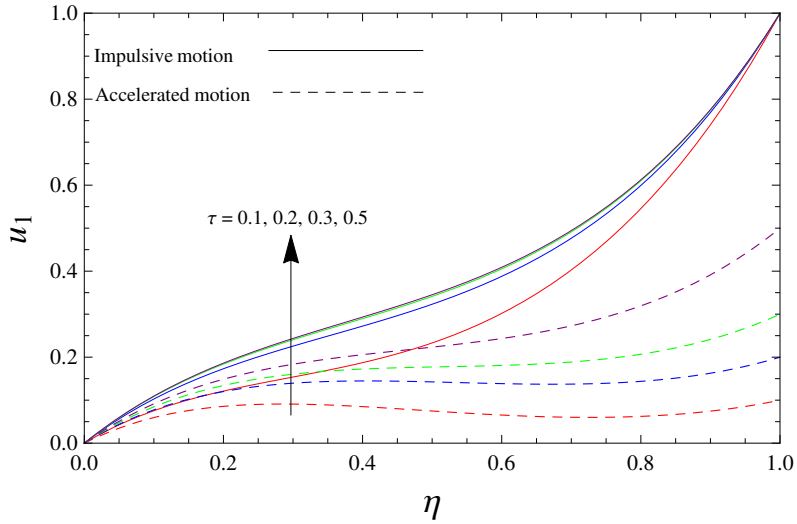

Fig.6.2(k): *Primary velocity profiles* u_1 *varying* τ *when* $N = 2$, $m = 0.5$, $M^2 = 10$, $Gr = 5$ *and* $Pr = 0.71$

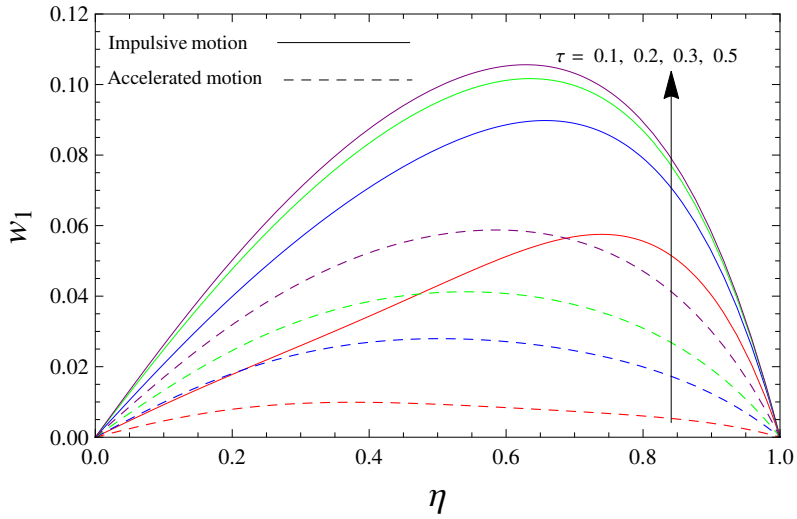

Fig.6.2(l): *Secondary velocity profiles* w_1 *varying* τ *when* $N = 2$, $m = 0.5$, $M^2 = 10$, $Gr = 5$ *and* $Pr = 0.71$

Figs.6.2(k) and 6.2(l), it is illustrated that the velocity components substantially increase when time τ progresses for both the impulsive as well as accelerated motions of the right wall of the channel. Fig.6.2 also focuses on the comparative analysis of impulsive motion and accelerated motion of the moving wall of the channel by varying flow parameters. The graphs explicate that both the velocity components for impulsive motion are always greater than the accelerated motion of the right wall of the channel.

Fig.6.3 displays the time evolution of the primary and secondary velocity profiles across the channel for a fixed set of parameter values from the time where the fluid is begun to flow. The primary velocity enhances from its value at the left wall to its value at the right wall which is moving impulsively [Figs. 6.3(a) and 6.3(b)].

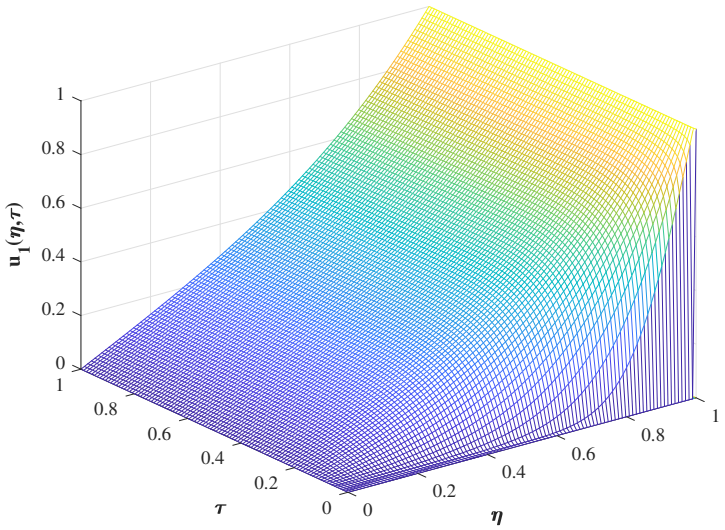

Fig.6.3(a): *Time evolution of u_1-profiles varying η and τ for impulsive motion*

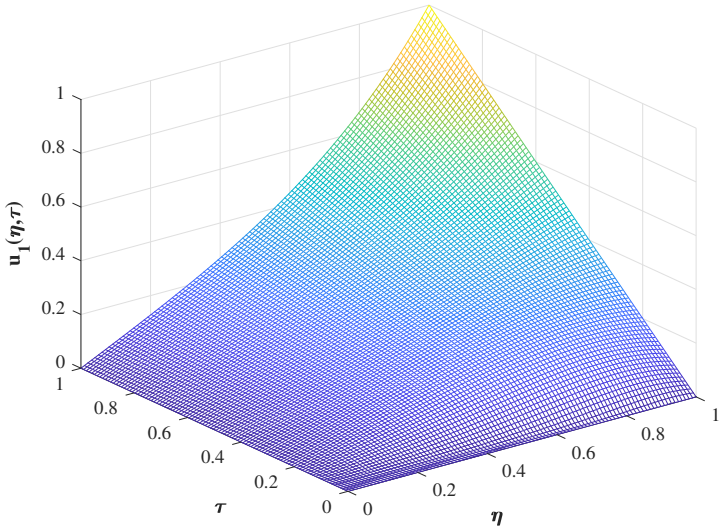

Fig.6.3(b): *Time evolution of u_1-profiles varying η and τ for accelerated motion*

In Figs.6.3(c) and 6.3(d), the secondary velocity is seen to increase from its prescribed value at the left wall to its maximum value attained in case of accelerated start of the moving right wall.

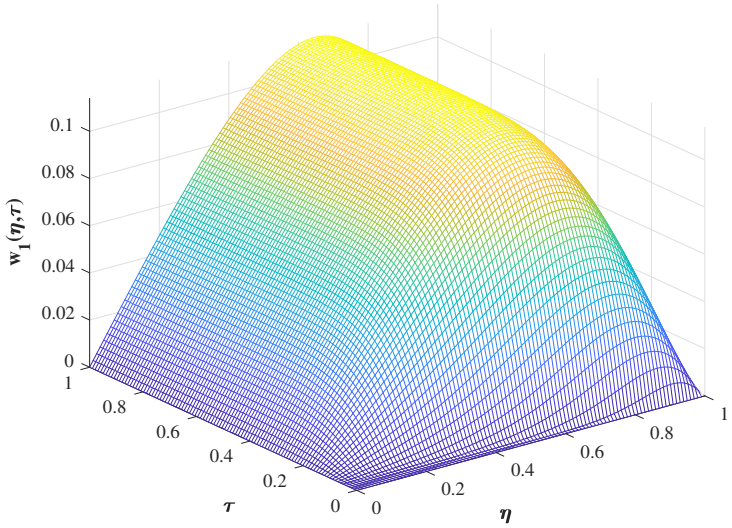

Fig.6.3(c): *Time evolution of w_1-profiles varying η and τ for impulsive motion*

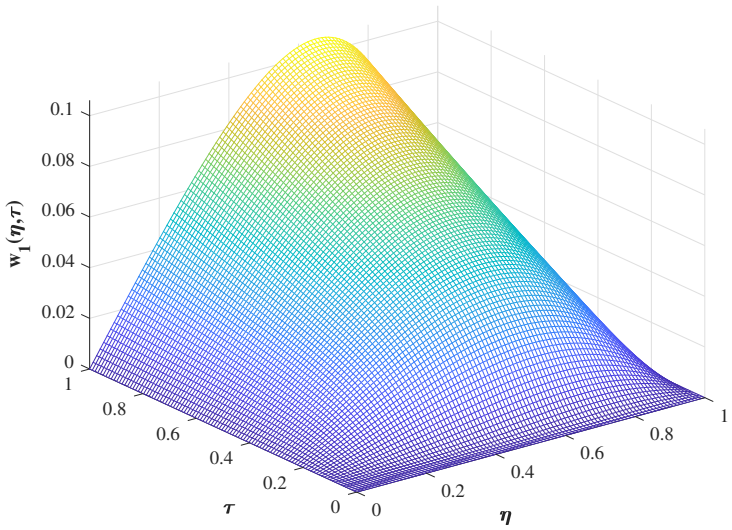

Fig.6.3(d): *Time evolution of w_1-profiles varying η and τ for accelerated motion*

6.3.2 Temperature profiles

Fig.6.4(a) portrays the effect of radiation parameter N on temperature profiles. The temperature profiles decrease as N increases, because the higher values of radiation parameter increase the absorption coefficient (K_{λ_w}) at the channel walls which therefore reduces the divergence of radiation heat flux $\frac{\partial q_r}{\partial y}$ leading to the reduced dissipation of kinetic energy as thermal energy. Therefore, temperature in fluid is reduced with lesser Joule dissipation. Thus, it is pointed out that the radiation effect induces cooling at a

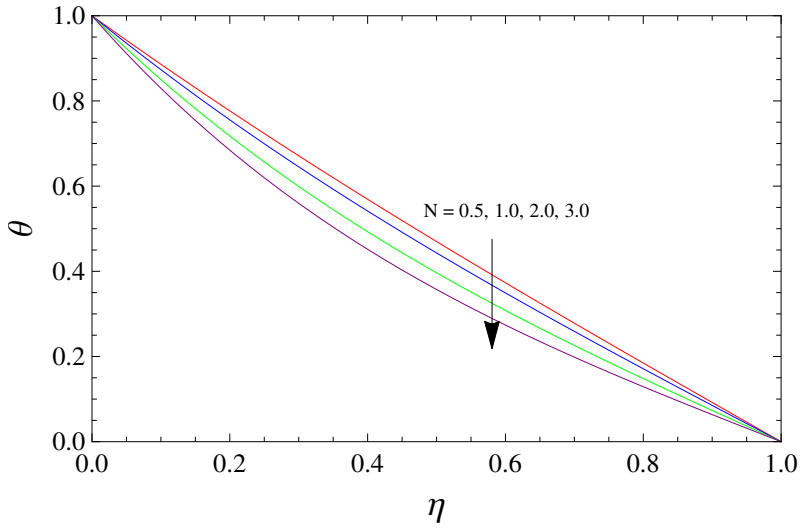

Fig.6.4(a): *Temperature profiles varying N when $Pr = 0.71$ and $\tau = 0.5$*

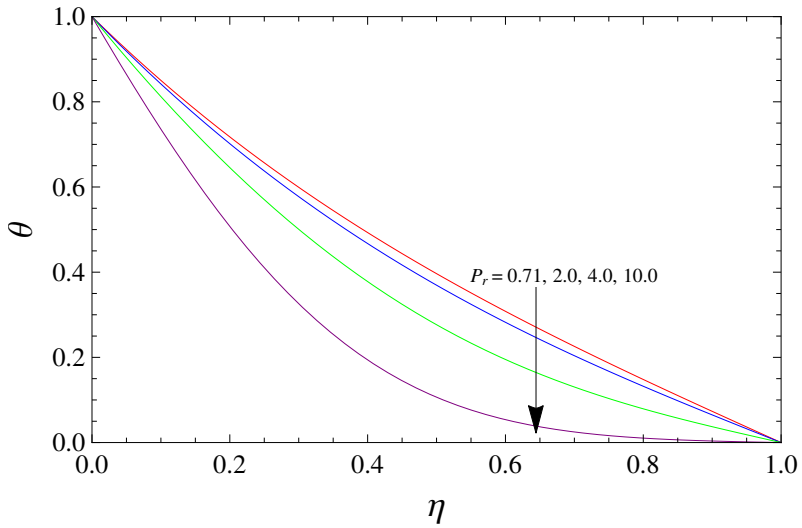

Fig.6.4(b): *Temperature profiles varying Pr when $N = 2$ and $\tau = 0.5$*

faster rate in the hydromagnetic channel flow regime. Fig.6.4(b) is aimed to shed light on the effect of Prandtl number Pr on temperature profiles. This figure explicates that Prandtl number reduces temperature substantially. This is related to the fact that there would be a decrease in temperature with the increase of Prandtl number.

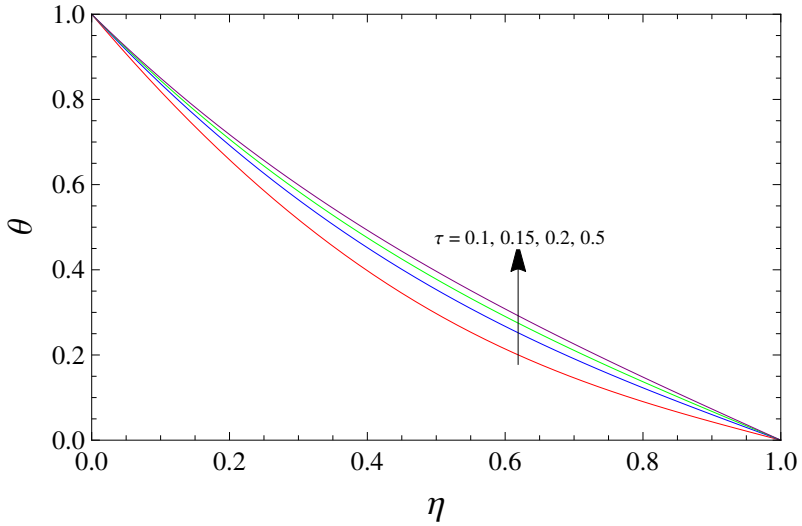

Fig.6.4(c): *Temperature profiles varying* τ *when* $N = 2$ *and* $Pr = 0.71$

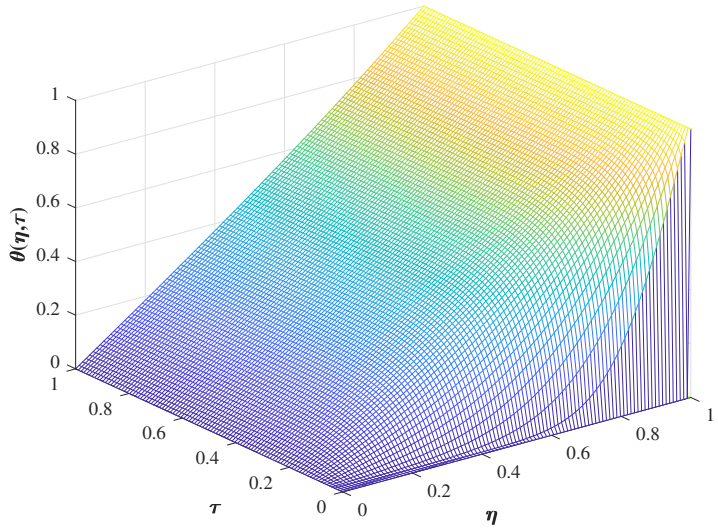

Fig.6.4(d): *Time evolution of temperature profiles varying* η *and* τ *when* $N = 2$ *and* $Pr = 0.71$

From Fig.6.4(c), it is noticed that as time τ progresses, there is an enhancement in temperature profiles. Fig.6.4(d) displays the time evolution of temperature profiles across the channel for a fixed set of parameter values from the time where the fluid is begun to flow. The temperature increases to its maximum value subject to the boundary conditions considered.

6.3.3 Shear stresses

For impulsive motion, the non-dimensional shear stresses τ_x and τ_z due to the primary and secondary flows at the fixed left wall of the channel ($\eta = 0$) are calculated from (6.28) and given by

$$\tau_x + i\,\tau_z = \frac{\partial q}{\partial \eta}\Big)_{\eta=0}$$

$$= \begin{cases} \frac{\sqrt{a}}{\sinh\sqrt{a}} + \frac{Gr}{(Pr-1)\alpha}\left(\sqrt{N}\coth\sqrt{N} - \sqrt{a}\coth\sqrt{a}\right) \\ +2\sum\limits_{n=0}^{\infty} n^2\pi^2\Bigg[(-1)^n\,\frac{e^{-\left(a+n^2\pi^2\right)\tau}}{(a+n^2\pi^2)} \\ +\frac{Gr}{Pr-1}\left\{\frac{e^{-\left(a+n^2\pi^2\right)\tau}}{(a+n^2\pi^2)(a-\alpha+n^2\pi^2)} - \frac{e^{-\left(N+n^2\pi^2\right)\frac{\tau}{Pr}}}{(N+n^2\pi^2)\left\{\frac{1}{Pr}(N+n^2\pi^2)-\alpha\right\}}\right\}\Bigg] & \text{for } Pr \neq 1 \\ \\ \frac{\sqrt{a}}{\sinh\sqrt{a}} + \frac{Gr}{(N-a)}\left(\sqrt{N}\coth\sqrt{N} - \sqrt{a}\coth\sqrt{a}\right) \\ -2\sum\limits_{n=0}^{\infty} n^2\pi^2\left[\left\{\frac{Gr}{N-a} - (-1)^n\right\}\frac{e^{-\left(a+n^2\pi^2\right)\tau}}{(a+n^2\pi^2)} - \frac{Gr}{N-a}\,\frac{e^{-\left(N+n^2\pi^2\right)\tau}}{(N+n^2\pi^2)}\right] & \text{for } Pr = 1. \end{cases} \tag{6.32}$$

For accelerated motion, the non-dimensional shear stresses τ_x and τ_z at the fixed left wall of the channel ($\eta = 0$) due to the primary and secondary flows are computed from (6.30) and expressed as

$$\tau_x + i\,\tau_z = \frac{\partial q}{\partial \eta}\Big)_{\eta=0}$$

$$= \begin{cases} \frac{\sqrt{a}}{\sinh\sqrt{a}}\tau + \frac{Gr}{(Pr-1)\alpha}\left(\sqrt{N}\coth\sqrt{N} - \sqrt{a}\coth\sqrt{a}\right) \\ + \frac{1}{2\sqrt{a}\sinh\sqrt{a}}\left(1 - \sqrt{a}\coth\sqrt{a}\right) \\ -2\sum\limits_{n=0}^{\infty} n^2\pi^2 \left[(-1)^n \frac{e^{-\left(a+n^2\pi^2\right)\tau}}{\left(a+n^2\pi^2\right)^2} \right. \\ \left. - \frac{Gr}{Pr-1}\left\{ \frac{e^{-\left(a+n^2\pi^2\right)\tau}}{(a+n^2\pi^2)(a-\alpha+n^2\pi^2)} - \frac{e^{-\left(N+n^2\pi^2\right)\frac{\tau}{Pr}}}{(N+n^2\pi^2)\left\{\frac{1}{Pr}(N+n^2\pi^2)-\alpha\right\}} \right\} \right] & \text{for } Pr \neq 1 \\ \frac{\tau\sqrt{a}}{\sinh\sqrt{a}} + \frac{Gr}{(N-a)}\left(\sqrt{N}\coth\sqrt{N} - \sqrt{a}\coth\sqrt{a}\right) \\ + \frac{1}{2\sqrt{a}\sinh\sqrt{a}}\left(1 - \sqrt{a}\coth\sqrt{a}\right) \\ -2\sum\limits_{n=0}^{\infty} n^2\pi^2 \left[(-1)^n \frac{e^{-\left(a+n^2\pi^2\right)\tau}}{\left(a+n^2\pi^2\right)^2} \right. \\ \left. + \frac{Gr}{N-a}\left\{ \frac{e^{-\left(a+n^2\pi^2\right)\tau}}{(a+n^2\pi^2)} - \frac{e^{-\left(N+n^2\pi^2\right)\tau}}{(N+n^2\pi^2)} \right\} \right] & \text{for } Pr = 1. \end{cases} \tag{6.33}$$

The numerical values of the non-dimensional shear stresses τ_x and τ_z at the left wall of the channel ($\eta = 0$) due to the primary and secondary flows are presented in Fig.6.5 for several values of M^2, m, N, Gr, Pr and time τ. The impact of squared-Hartmann number M^2 on the shear stresses is disseminated in Figs.6.5(a) and 6.5(b). As M^2 increases, both the shear stresses τ_x and τ_z are reduced for both cases of impulsive and accelerated motions.

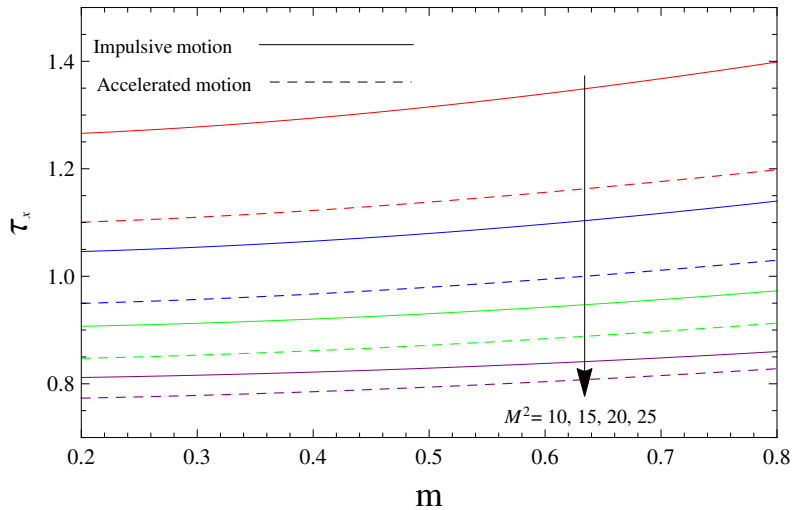

Fig.6.5(a): *Shear stress τ_x varying M^2 when $N = 2$, $Gr = 5$, $Pr = 0.71$ and $\tau = 0.5$*

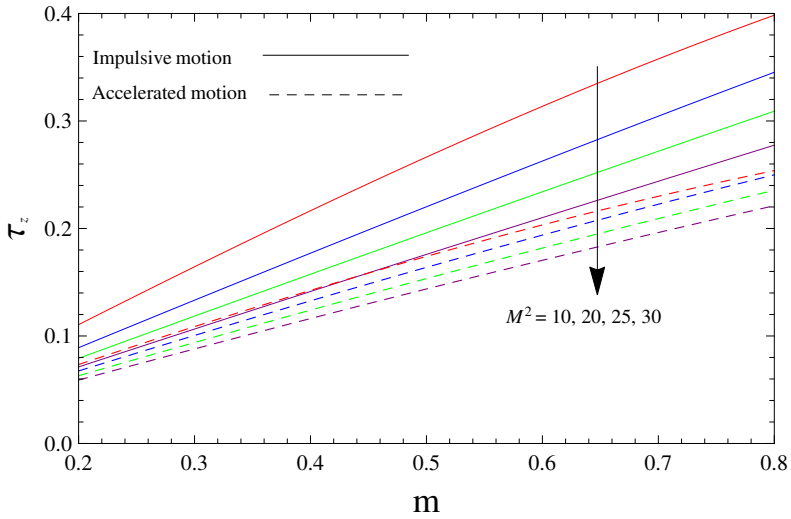

Fig.6.5(b): *Shear stress* τ_z *varying* M^2 *when* $N = 2$, $Gr = 5$, $Pr = 0.71$ *and* $\tau = 0.5$

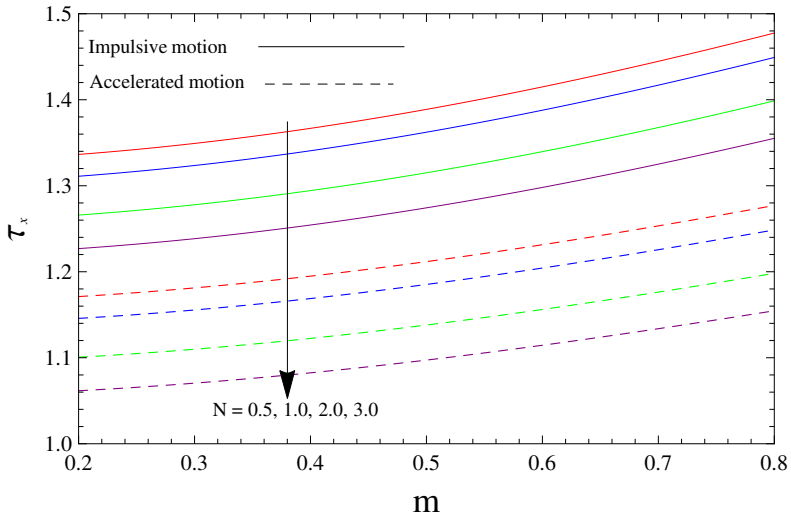

Fig.6.5(c): *Shear stress* τ_x *varying* N *when* $Gr = 5$, $Pr = 0.71$, $M^2 = 10$ *and* $\tau = 0.5$

Figs.6.5(c) and 6.5(d) show that radiation parameter N has a tendency to reduce the shear stresses τ_x and τ_z at the wall $\eta = 0$ for both cases of the impulsive as well as accelerated motions of the right wall of the channel.

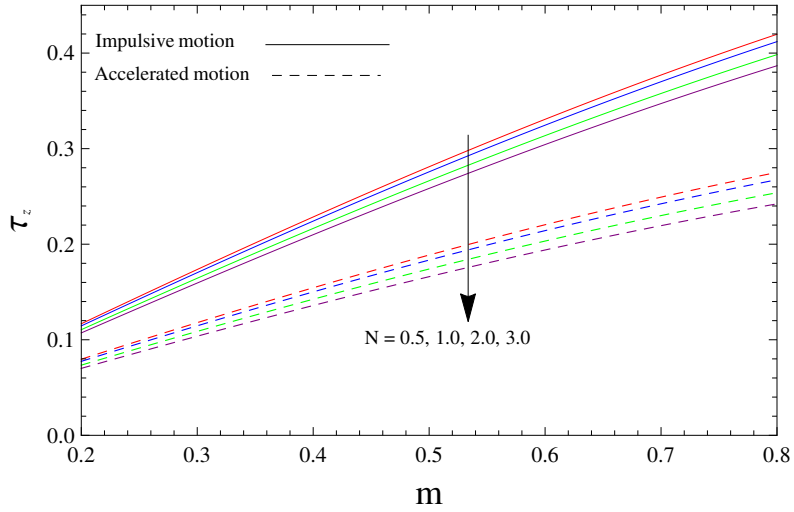

Fig.6.5(d): *Shear stress* τ_z *varying* N *when* $Gr = 5$, $Pr = 0.71$, $M^2 = 10$ *and* $\tau = 0.5$

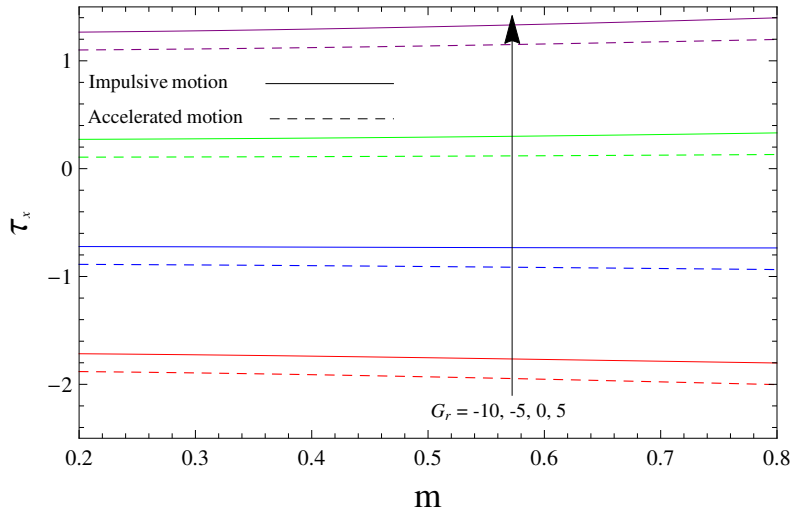

Fig.6.5(e): *Shear stress* τ_x *varying* Gr *when* $N = 2$, $Pr = 0.71$, $M^2 = 10$ *and* $\tau = 0.5$

It is illustrated from Figs.6.5(e) and 6.5(f) that the shear stresses τ_x and τ_z boost up with increasing Gr for both the impulsive as well as accelerated motions of the wall $\eta = 1$.

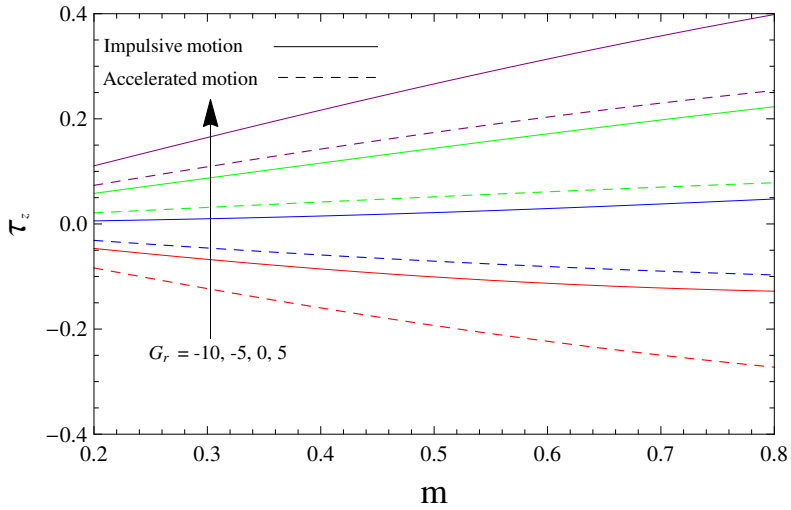

Fig.6.5(f): *Shear stress* τ_z *varying* Gr *when* $N = 2$, $Pr = 0.71$, $M^2 = 10$ *and* $\tau = 0.5$

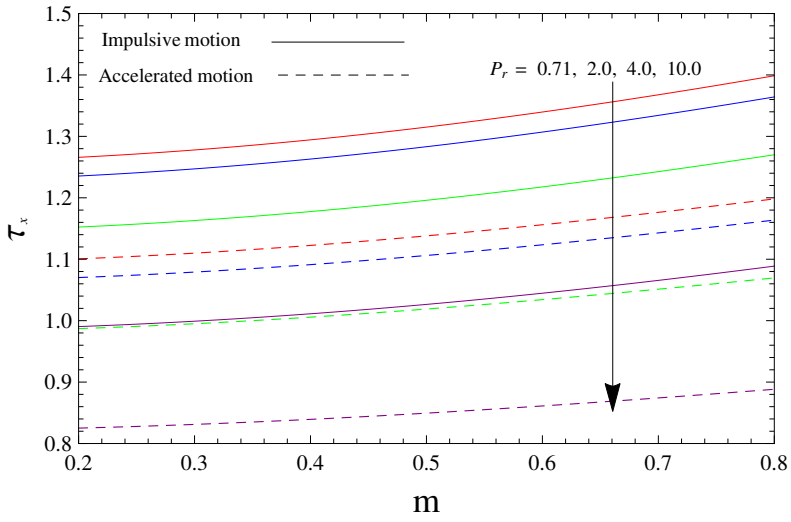

Fig.6.5(g): *Shear stress* τ_x *varying* Pr *when* $N = 2, Gr = 5, M^2 = 10$ *and* $\tau = 0.5$

Figs.6.5(g) and 6.5(h) show that the shear stresses τ_x and τ_z reduce for increasing values of Pr for both prescribe motions of the right wall. Physically, it is possible because fluids with Prandtl number move slowly and hence there is more friction at the channel walls.

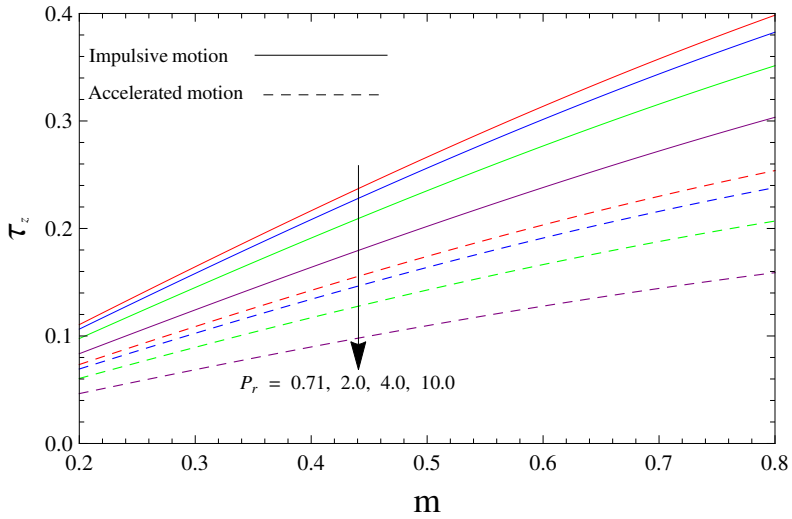

Fig.6.5(h): *Shear stress* τ_z *varying* Pr *when* $N = 2, Gr = 5, M^2 = 10$ *and* $\tau = 0.5$

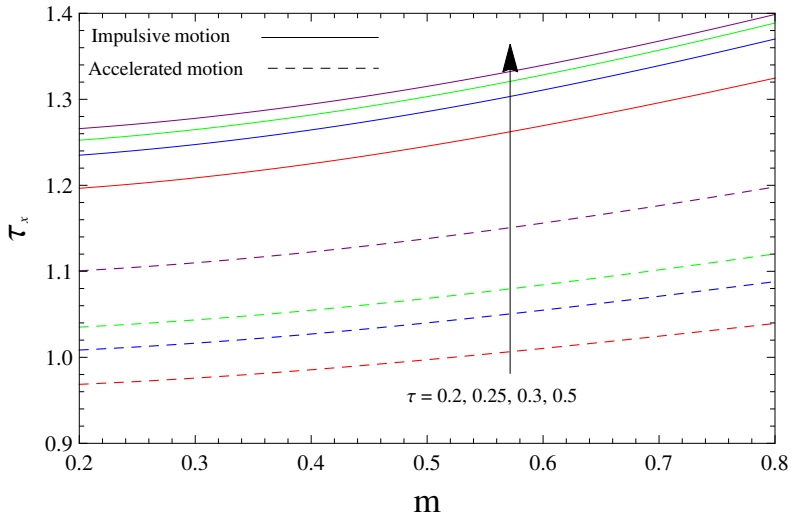

Fig.6.5(i): *Shear stress* τ_x *varying* τ *when* $N = 2$, $Gr = 5$, $Pr = 0.71$ *and* $M^2 = 10$

The time parameter τ has increasing affect on both shear stresses τ_x and τ_z for both motions [Figs.6.5(i) and 6.5(j)]. Further, it is observed from Fig.6.5 that the shear stresses at the left wall ($\eta = 0$) of the channel, in case of impulsive start of moving wall is greater than accelerated start of the right wall of the channel.

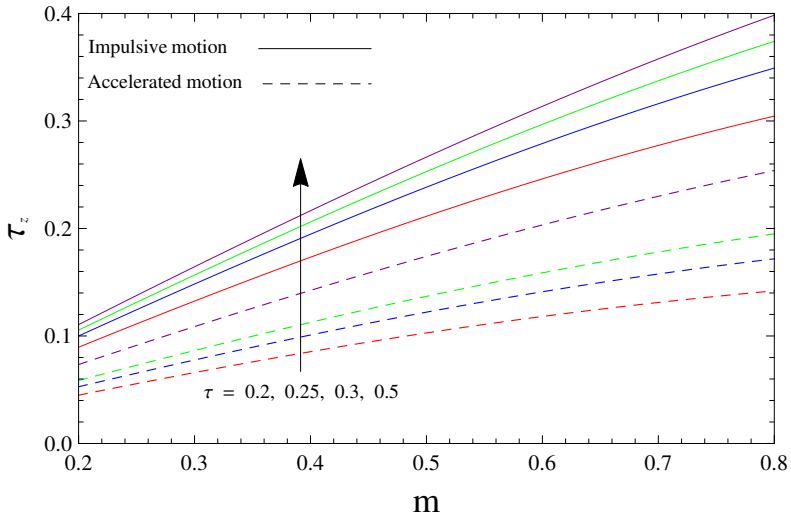

Fig.6.5(j): *Shear stress* τ_z *varying* τ *when* $N = 2$, $Gr = 5$, $Pr = 0.71$ *and* $M^2 = 10$

6.3.4 Rate of heat transfer

For engineering point of view, the rate of heat transfer is a quantity of foremost interest. The expression of the rate of heat transfer governing the heat transfer characteristics at the channel walls ($\eta = 0,\ 1$) are calculated from (6.27) and given by

$$\begin{aligned} -\theta'(0) &= -\frac{\partial\theta}{\partial\eta}\Big)_{\eta=0} \\ &= \sqrt{N}\coth\sqrt{N} + 2\sum_{n=0}^{\infty}\frac{n^2\pi^2}{(N+n^2\pi^2)}e^{-(N+n^2\pi^2)\frac{\tau}{Pr}}, \qquad (6.34) \\ -\theta'(1) &= -\frac{\partial\theta}{\partial\eta}\Big)_{\eta=1} \\ &= \frac{\sqrt{N}}{\sinh\sqrt{N}} + 2\sum_{n=0}^{\infty}(-1)^n\frac{n^2\pi^2}{(N+n^2\pi^2)}e^{-(N+n^2\pi^2)\frac{\tau}{Pr}}. \qquad (6.35) \end{aligned}$$

The numerical values of the rate of heat transfer $-\theta'(0)$ and $-\theta'(1)$ are plotted in Fig.6.6 for several values of physical parameters, viz. N, Pr and τ. Fig.6.6(a) portrays the variation of the rate of heat transfer at the channel walls with respect to Prandtl number Pr. The rate of heat transfer $-\theta'(0)$ at the left wall of the channel($\eta = 0$) is enhanced and $-\theta'(1)$ at the right moving wall of the channel($\eta = 1$) is reduced by increasing Pr. Prandtl number signifies the ratio of momentum diffusivity to thermal diffusivity. Fluids with lower Prandtl number will possess higher thermal conductivities so that heat can diffuse from the left wall ($\eta = 0$) faster than for higher Pr fluids.

Hence, Prandtl number can be used to increase the rate of cooling in conducting flows.

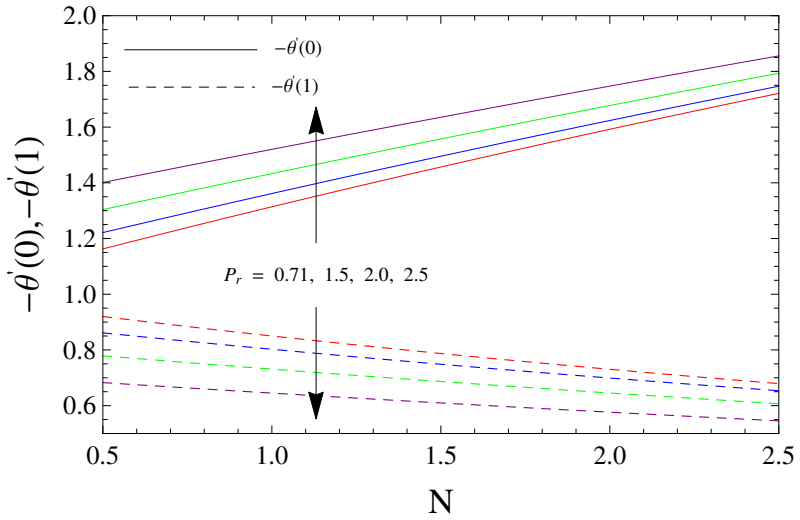

Fig.6.6(a): *Rate of heat transfer varying Pr when* $\tau = 0.5$

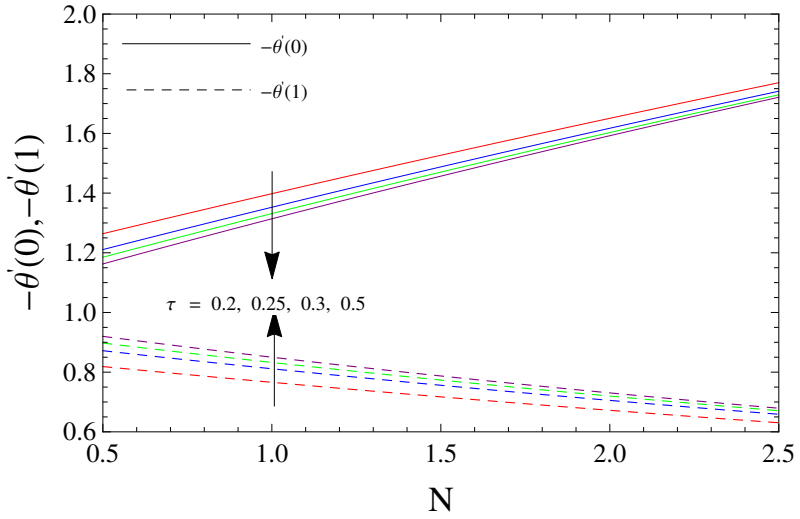

Fig.6.6(b): *Rate of heat transfer varying* τ *when* $Pr = 0.71$

In Fig.6.6(b), the rate of heat transfer $-\theta'(0)$ reduces whereas the rate of heat transfer $-\theta'(1)$ enhances as time τ progresses. The rate of heat transfer at both channel walls is negative for all parameter, which means that the heat is always transferred from the channel walls to fluid.

6.4 Conclusion

In the present study, an analytical investigation has been presented to expose the impact of Hall current effects on unsteady MHD convective flow and heat transfer of a viscous incompressible electrically conducting fluid in a moving vertical channel adopting Cogley-Vincent-Gilles heat flux model. Employing Laplace transform technique, the governing equations are solved. Closed form expressions for the fluid velocity components, temperature, shear stresses and the rate of heat transfer at the channel walls are obtained. Emphasis is given on how flow dynamics are changed due to the effect of the strong magnetic field along with Hall currents. The key findings of the present study are highlighted below:

- The velocity components are declined due to increasing values of the magnetic field or radiation parameter.
- Increasing Hall parameter strongly accelerates the velocity components.
- The buoyancy force significantly enhances the fluid velocity components throughout the channel.
- An enhancement in thermal radiation parameter leads to cooling of fluid.
- The wall shear stresses are significantly increased by increasing Hall parameter.
- The wall shear stresses are reduced by increasing radiation parameter.
- As time progresses there is an enhancement in the rate of heat transfer at the moving channel walls.
- Inclusion of Hall currents exerts a profound influence on the flow characteristics.